

UNIVERSIDADE ESTADUAL DE CAMPINAS  
SISTEMA DE BIBLIOTECAS DA UNICAMP  
REPOSITÓRIO DA PRODUÇÃO CIENTÍFICA E INTELLECTUAL DA UNICAMP

**Versão do arquivo anexado / Version of attached file:**

Versão do Editor / Published Version

**Mais informações no site da editora / Further information on publisher's website:**

[https://pubs.acs.org/doi/abs/](https://pubs.acs.org/doi/abs/10.1021/jp509574s)  $\text{W.}$   $\text{\%o}$

**DOI: 10.1021/jp509574s**

**Direitos autorais / Publisher's copyright statement:**

©2014 by American Chemical Society. All rights reserved.

DIRETORIA DE TRATAMENTO DA INFORMAÇÃO

Cidade Universitária Zeferino Vaz Barão Geraldo

CEP 13083-970 – Campinas SP

Fone: (19) 3521-6493

<http://www.repositorio.unicamp.br>



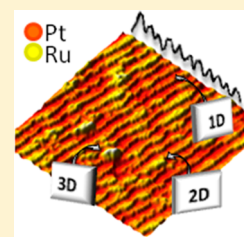
# From 1D to 3D Ru Nanostructures on a Pt Stepped Surface as Model Systems in Electrocatalysis: UHV-STM and XPS Study

Emilia A. Carbonio,\* Mauricio J. Prieto,\* Abner de Siervo, and Richard Landers

Departamento de Física Aplicada, Instituto de Física Gleb Wataghin, Universidade Estadual de Campinas, 13083-859 Campinas, SP, Brazil

## Supporting Information

**ABSTRACT:** A Ru-decorated Pt single crystal vicinal to the (111) plane was studied using scanning tunneling microscopy (STM) and X-ray photoemission spectroscopy (XPS) in ultrahigh-vacuum environment. Pt(332) vicinal surface was used, and different coverages of Ru ( $\theta_{\text{Ru}}$ ) were deposited. STM images show that Ru initial growth is highly influenced by the stepped nature of the surface. For instance, 1D and 2D nanostructures grow decorating the steps at low coverage ( $\theta = 0.34$ ), while at higher coverage a second layer is stabilized and bilayer (3D) growth sets in. The size and shape of the Ru nanostructures differ from those reported for Ru on Pt(111) due to the high density of steps that induces anisotropic growth and delays the monolayer to bilayer growth transition. Sample annealing at 623 K promotes further anisotropy and an increase in the amount of 3D structures. XPS suggests that no bulk alloying (bulk diffusion) of Ru occurs at this temperature. Additionally, our findings are used to discuss the different electrocatalytic behavior reported for some Pt–Ru systems and to explain tendencies observed for Ru-decorated Pt nanoparticles toward the  $\text{CH}_3\text{OH}$  and CO electrooxidation reactions.



## INTRODUCTION

The shape and surface structure of catalysts are important factors in determining their catalytic activity, since many reactions of interest for fuel cells applications are structure-sensitive.<sup>1–4</sup> Furthermore, bimetallic materials have shown superior catalytic activity as both cathode and anode materials.<sup>5,6</sup> Particularly interesting are Pt–Ru containing systems which have been shown, over the past decades, to have the best catalytic activity and stability toward the electrooxidation reactions related to direct methanol fuel cells (DMFCs).<sup>6–8</sup>  $\text{CH}_3\text{OH}$  complete oxidation to  $\text{CO}_2$  can occur by different paths simultaneously. In a simplified vision, two paths can be described: the direct (preferred) path where soluble intermediates are formed (formic acid and formaldehyde) and the (unwanted) poisoning path for which  $\text{CO}_{\text{ads}}$  is formed.<sup>8,9</sup> In this respect, catalysts are required not only to improve the kinetics of the Methanol oxidation reaction (MOR) but also to be able to oxidize  $\text{CO}_{\text{ads}}$ . The enhancement of the electrocatalytic activity of Ru–Pt alloys and decorated surfaces (Pt/Ru and Ru/Pt) toward MOR has been attributed to two different factors:<sup>8</sup> (i) the electronic effect due to changes in the Pt d-band vacancy<sup>10–12</sup> and (ii) a bifunctional mechanism, where Ru provides activated water species necessary to oxidize carbon-containing species.<sup>12–14</sup> However, the exact means of activity enhancement for this system is still a topic of debate, and there are still unanswered questions. This has stimulated over the past decades the study of the physical reasons for the enhanced activity.<sup>8</sup>

Extensive research on the MOR has been conducted with nanoparticles (NPs),<sup>15–20</sup> single crystals,<sup>21–24</sup> and theoretical calculations.<sup>10,11,25</sup> However, significant understanding came with the development of techniques that allowed studying well-

defined surfaces prepared in UHV conditions, and these have become attractive model systems since then. Because catalytic properties of NPs can change with shape, particle size, and composition, it becomes difficult to separate each contribution. Thus, the modifications of Pt and Ru low-Miller-index single crystals with Ru and Pt, respectively, have been studied and well characterized as model systems over the past years with techniques such as photoelectron spectroscopy and UHV-STM, among others.<sup>26–32</sup> However, catalysts consisting of NPs, which are used at fuel cells, do not always have the same behavior as these single crystals. Electrochemical characterization of methanol and carbon monoxide electrooxidation has also been reported using vicinal surfaces.<sup>2,3,33,34</sup> A vicinal surface consists of a single crystal whose surface normal is tilted by a few degrees with respect to the normal of a basal plane, giving rise to surfaces with a terrace-step structure with a defined terrace width and a high density of steps<sup>35</sup> that may resemble better NPs surfaces. For instance, step sites in Pt electrodes were shown to promote dissociative adsorption of methanol at lower potentials (in the classical hydrogen adsorption region), which is inhibited for low-Miller-index single crystals,<sup>3,34</sup> and to increase the oxidation rate.<sup>2</sup>

On the other hand, surfaces with high density of defects have been very little explored as model systems for studying the growth and structure of bimetallic surfaces of catalytic interest using UHV-STM.<sup>36,37</sup> Hoster et al.<sup>26</sup> studied the effect of surface defects on the catalytic activity and observed higher MOR activity for a sputtered Pt–Ru bulk alloy compared to

**Received:** September 22, 2014

**Revised:** November 7, 2014

**Published:** November 18, 2014



smooth surfaces, but as mentioned by the authors, that surface has the disadvantage that its structure cannot be assessed by STM. In this respect, decorated vicinal surfaces can be used as model systems and offer the possibility of studying structure effects induced by high density of well-characterized defects. Additionally, much progress has been done in controlling NPs shape and size, and over the past years NPs having high index facets have been successfully prepared.<sup>38–42</sup> This requires new model systems, which might resemble better the surface of these new NPs. Here again, vicinal surfaces as model systems could bring new insights to correlate the structure–activity relation.

Here we present a study of the structure of Ru-decorated Pt(332) vicinal surface. The Pt(332) vicinal surface consists in terraces (of (111) orientation) having six atomic rows wide and monatomic steps. To the best of our knowledge, there is no UHV-STM structure study reported on any Ru-decorated vicinal Pt surface. We study how the high density of steps affects the initial growth and final surface structure, considering the surface processes involved at the initial growth. Also, XPS is used for all samples to evaluate alloy formation and segregation. Our results are compared with those reported for Ru-decorated low-Miller-index single crystals. Also, we investigate the effect of annealing the surface at 623 K. Finally, the implications of the differences observed for the vicinal surface in the present research compared to low-Miller-index surfaces are discussed in terms of the electrocatalytic activity of methanol and carbon monoxide oxidation reported in the literature for single crystals and NPs.

## EXPERIMENTAL SECTION

All experiments were carried out in an ultrahigh-vacuum (UHV) system. The chamber is equipped with a SPECS-Phoibus 150 hemispherical electron analyzer with nine-channeltron detection, an argon ion gun for sputtering, a water-cooled evaporator, and a high precision two rotation axis manipulator, allowing sample transfer and heating up to 1200 K by electron bombardment. The setup operates in a base pressure better than  $5 \times 10^{-10}$  mbar regime during evaporation and measurements. The XPS experiments were performed using an Al K $\alpha$  source. All photoelectron spectra were collected at 60° from the surface normal. Additionally, the sample could be transferred directly to an adjoining chamber equipped with an Aarhus 150 (SPECS) scanning tunneling microscope (STM) operating under UHV, available for STM measurements with a tungsten tip in constant current mode and room temperature (RT). The operating base pressure during image acquisition was always in the  $10^{-11}$  mbar range. WSxM<sup>43</sup> software was used for image processing. Ru coverage ( $\theta_{\text{Ru}}$ ) was calculated from the Pt 4f core-line attenuation and calibrated with STM.

The Pt single crystal was obtained from Mateck GmbH as a 10 mm diameter hat-shaped disk oriented in the (332) direction, i.e., a surface with a miscut angle of 10° with respect to the [111] direction and along the [11–2] direction. The orientation accuracy is better than 0.1°. The surface was thoroughly cleaned prior to Ru deposition using consecutive cycles of sputtering and annealing. Sputtering was performed using 1 keV Ar<sup>+</sup> ions for short periods of time (typically 10–15 min) followed by annealing in O<sub>2</sub> and UHV consecutively, at 923 and 1023 K, respectively, in order to regenerate the surface. XPS measurements were performed between cycles to follow oxygen and carbon 1s photoelectron lines in order to ensure

the effectiveness of the cleaning methodology. Once a clean surface was achieved, STM and XPS measurements were performed, and Ru was deposited from a pure Ru pellet contained in a W basket, at constant rate and the substrate at RT. Deposition time was varied in order to obtain different coverage, in the range  $\theta_{\text{Ru}} = 0.34\text{--}1.48$  ML. Deposits were investigated using XPS and STM. Finally, the effect of annealing at 623 K (for 5 min) was studied.

## RESULTS AND DISCUSSION

Initially, the Pt(332) surface was characterized prior to Ru deposition. Figure 1 shows a STM image and the X-ray

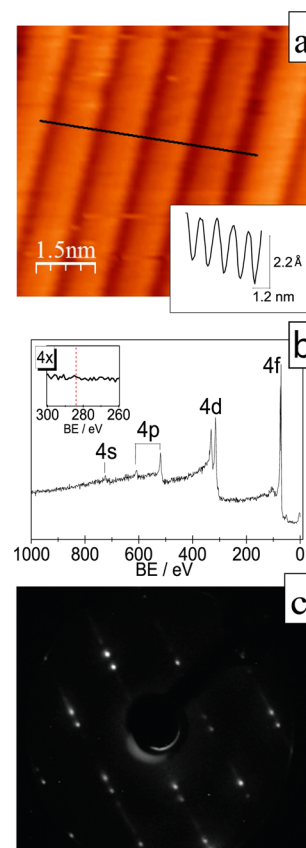


**Figure 1.** (a) STM image ( $6 \text{ nm} \times 7 \text{ nm}$ ) of the clean Pt(332) surface.  $U_b = 1.06 \text{ V}$ ,  $I_t = 0.8 \text{ nA}$ . Inset: line profile across terraces. (b) X-ray photoelectron spectra of the clean surface shown in (a), measured at 60° from surface normal. Inset: magnification of the spectra at the C 1s BE (red line). (c) LEED pattern obtained at 155 eV. All measurements were done at RT conditions.

photoelectron spectra of the clean surface. From Figure 1a is possible to see the stepped nature of the Pt(332) surface. The line profile showing the topography of the surface is displayed also in the figure (inset). The mean value of the terrace width was determined to be  $12.4 \pm 0.1 \text{ Å}$ , in agreement with the theoretical value,  $12.8 \text{ Å}$ , calculated for the hard sphere model of a stepped surface proposed by Clavillier et al.<sup>44</sup> The mean height of the monatomic steps was found to be  $2.2 \text{ Å}$  (close to the value of  $2.27 \text{ Å}$  for a Pt(111) step).<sup>29</sup>

The X-ray photoelectron spectra (Figure 1b) shows only the main core lines for Pt, confirming the efficiency of the cleaning procedure. LEED pattern (Figure 1c) confirms the ordered stepped nature of the surface, as it reveals well-defined spots representative of long-range order at the surface. The pattern

consists of regular 3-fold symmetry spots corresponding to the (111) plane and regularly spaced satellite spots generated by the periodic steps at the surface. The calculated ratio  $d_{\text{Pt-Pt}}/W_{\text{terrace}}$  in the reciprocal lattice space agrees well with the expected value for a Pt(332) surface.

Figure 2 shows the X-ray photoelectron spectra for the deposition of Ru on Pt(332) in the range  $\theta_{\text{Ru}} = 0.34$ –1.48 ML.

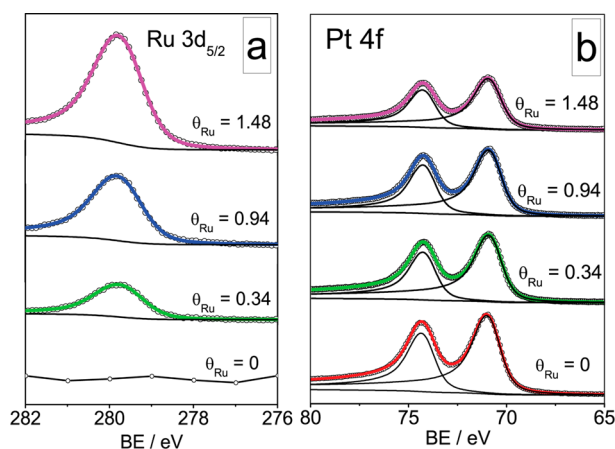


**Figure 2.** XPS of Ru 3d<sub>5/2</sub> and Pt 4f core level lines as a function of Ru coverage in ML (as indicated in the figure) measured at RT, at 60° of surface normal. Fitting was done using a Shirley function for background and Doniach–Sunjic function for all core lines.

The Ru 3d<sub>5/2</sub> core-line has a binding energy (BE) of 279.6 eV, which is independent of the coverage, and corresponds to metallic Ru.<sup>45</sup> Ru BE has already been observed to be independent of coverage when deposited on Pt(111).<sup>46</sup> The BE of Pt 4f<sub>7/2</sub> core line for all samples is 70.7 eV. Parameters obtained from fitting are presented in Table 1S.

**Ru Growth. Low Coverage.** Figure 3 shows STM images of the Ru/Pt(332) surface for  $\theta_{\text{Ru}} = 0.34$  ML. From Figure 3a it can be seen that the stepped structure of the surface is maintained. In Figure 3b it can be seen that Ru appears as bright spots, which is due to chemical contrast.<sup>28,29,47</sup> Ru deposits at the step edges as evidenced from the figure. In the inset, the line profile of the atomically resolved 1D chain structure formed by Ru atoms at the step edge of the Pt substrate is shown. The estimated Ru–Ru distance is 2.9 Å (close to the value 2.77 Å for Pt–Pt in a (111) surface). Ad-islands, i.e. 2D structures, are also visible in the STM image.

Other authors observed fully decorated steps by bilayer islands (3D structures) for Ru deposition on Pt(111) at temperatures up to 303 K.<sup>26,29</sup> Brekó et al.<sup>29</sup> observed a tendency toward the formation of Ru islands with a bilayer height (~50% of the islands as bilayers) when Ru was grown on Pt(111) at 303 K at a Ru coverage of 0.4 ML. The authors suggested that the bilayer configuration is the thermodynamically favored one, but at 303 K bilayer formation would be kinetically hindered. We observe mainly the formation of 1D and 2D structures on Pt(332). Comparison between these two systems is reasonable since the Pt(332) terraces have the (111) orientation. Our results for Ru on the vicinal Pt surface indicate that the high density of surface steps (low coordinated atoms) affects the initial stage of island evolution due to the preference of the incoming ad-atoms to nucleate along the step edges.

The 1D and 2D structures formation can be rationalized considering the surface atomic processes that occur during

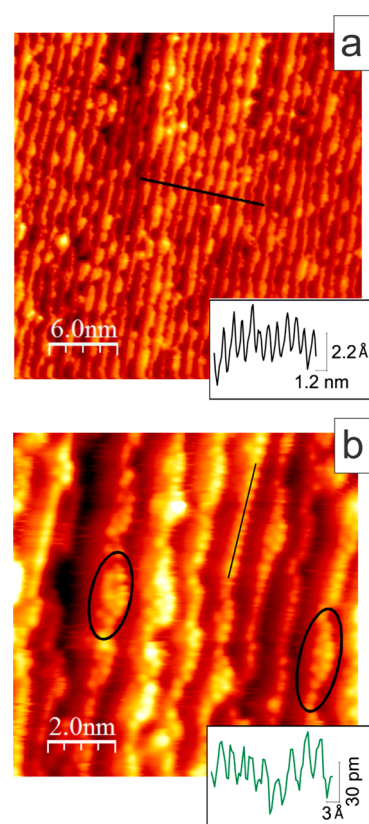


**Figure 3.** STM images at RT of the Ru<sub>0.34</sub>/Pt(332) surface. (a) 30 nm × 30 nm;  $U_b = 1.1$  V,  $I_t = 0.8$  nA and (b) 10 nm × 10 nm;  $U_b = 1.1$  V,  $I_t = 0.81$  nA. Inset in (a) shows the terrace profile. Inset in (b) shows the line profile of the atomically resolved 1D structure along the step edge.

film/cluster growth from the vapor phase. As the description of all possible surface processes is not the main objective of this publication, those considered relevant for the discussion of the results will be mentioned and briefly described. Readers interested in more details of surface processes may refer to refs 48–51.

During and after the deposition of the metal atoms on the surface, mainly diffusion processes take place. Atoms diffusing along the surface may encounter other atoms forming clusters or islands that can also diffuse or may encounter a step edge. The first case is generally the dominant process at low temperatures, large terrace size, and high adsorption rates.<sup>50</sup> In the present case of a vicinal surface, processes occurring at steps and kinks become important. As it is well-known, adsorbates have higher binding energy at step and kink sites;<sup>50</sup> thus, it is expected that step decoration occurs at the first stage of growth almost exclusively, as shown in Figure 4 (stage A). Because of the small size of the terraces, ad-atoms can reach a step and attach to it before another atom lands on the surface, preventing island growth on the terraces.<sup>49</sup>

Atoms attached to a step may be free to diffuse along the step edge, even at room temperature.<sup>48</sup> An atom reaching an already decorated step will attach to it; it may be incorporated to the previously formed row (undergoing a corner-diffusion process), or it may remain at the second row where it was first attached, depending on the activation energy required for the first process to occur<sup>50</sup> (Figure 4, stage B). In the latter case 2D ad-island growth is favored instead of 1D, as step edges start to roughen, and thus, the protruding parts can attach more



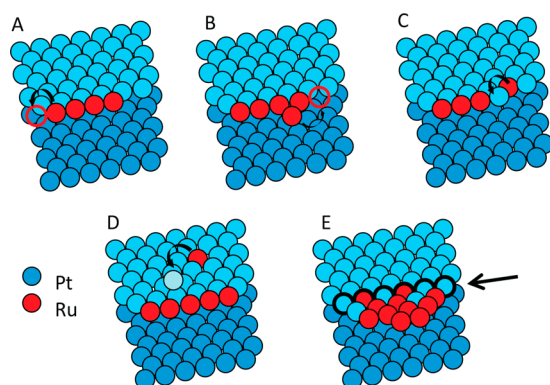


**Figure 4.** Schematic representation of surface processes for the initial growth of Ru on Pt(332). The unfilled red circles represent a site that could be occupied by the diffusion (curved arrows) of a Ru ad-atom. The black arrow in (E) indicates the original position of the step edge. See text for full description.

diffusing atoms than the recessed parts.<sup>50</sup> For Pt deposition on Pt (997) (a vicinal surface of the same family of Pt (332)), short 1D chains are formed in the temperature range of 300–400 K, whereas below 300 K, atoms become attached to a second row, suggesting that below 300 K the corner-diffusion process for Pt on Pt(997) is kinetically hindered.<sup>50</sup> In heteroepitaxy, this process is hindered below 175 K for Cu and below 250 K for Ag, Co, and Fe over Pt(997). For Mo, roughened ad-islands grow at least at temperatures up to 500 K.<sup>50</sup> From the STM images (Figure 3) of Ru/Pt(332) it can be seen that steps are almost fully decorated by 1D or 2D structures. The coverage of 0.34 ML corresponds approximately to two Ru atoms per Pt step atom. This means that for a row-by-row growth mode, steps would be fully decorated by two Ru atomic rows. Instead, 2D structures with two and more than two rows are observed along with 1D structures, at the step edges. Thus, we can conclude that at least after steps are fully decorated, and 2D structures begin to grow, corner diffusion is hindered and a third row of atoms can grow at the previously formed 2D ad-island. This is probably related to the rough shape of the 2D structures and the consequent increase of the binding energy of Ru atoms to the second atomic row, which consequently prevents the corner-diffusion process from occurring.

The saturation of the first atomic row before the beginning of 2D structures growth cannot be concluded from the preset measurements. Lower coverage of Ru could not be studied due to instrumental limitations. Complementary measurements using for example in-situ He reflectivity in grazing angle scattering geometry should help to address this issue.

In addition, from Figure 3b, ad-islands seem to be constituted by both Pt and Ru (see black ellipsis in Figure 3b). At this point it is worth mentioning that step decoration may take place exclusively from the lower terrace due to the presence of an Ehrlich–Schwöbel (ES) barrier, which reduces the attachment of an ad-atom diffusing from the upper terrace to the step (by hopping over the step). However, a diffusing atom can exchange with a descending step edge atom by insertion into the surface at the atomic layer behind the step edge atom, which will be pushed forward<sup>48,52</sup> (Figure 4C). Calculations for the self-diffusion on Pt(111)<sup>53,54</sup> and Rh(111)<sup>55</sup> gave higher energy barriers for the hopping against the exchange process on the step, so the hopping process was

considered negligible compared to the exchange process at the step<sup>53</sup> for those systems.

Furthermore, an exchange process can take place at the step edge (Figure 4C) and also at the terrace (Figure 4D). For Ni deposited on Pt (997) at 200 K, exchange processes are favored but not limited to step sites, and some Ni atoms can be observed at random positions at the terraces.<sup>36</sup> In our case, Ru atoms are observed exclusively at step edges and ad-islands, but not on the terraces. On the other hand, the exchange process at the terrace may require higher activation energy, and thus, it could take place depending on the substrate temperature during deposition.<sup>36,48</sup> The exchange of Ru atoms with Pt (111) surface atoms was proposed to begin at temperatures as low as 373 K from experimental observations.<sup>29</sup> At 573 K, islands were observed to be composed by both Ru and Pt atoms, but no Ru was observed by the authors at the uncovered terrace areas between the islands. They suggested that exchange takes place during growth at the perimeter of the growing island, while exchange process at the terrace could become more probable with increasing temperature.<sup>29</sup> Hence, in the present case of Ru/Pt(332), the exchange between Ru ad-atoms and the Pt substrate must be considered. Since islands grow exclusively attached to the steps (as seen from STM images), we suggest that at 298 K the exchange of Ru atoms with Pt atoms at the terrace must be kinetically hindered. Also, as Pt(332) has a small terrace width (12.4 Å) a diffusing ad-atom rapidly encounters a step site to attach to. For example, homoepitaxial growth on Pt(111) is dominated by the islands nucleation over the terrace and the rate of atom transfer between them; however, Pt diffusion on Pt(997), which has a terrace width of 20.1 Å, at temperatures above 80 K can be considered as fast as the interlayer diffusion due to the small size of the terraces.<sup>50</sup>

Ru has strong antisegregation at the dilute limit on the Pt(111) surface.<sup>56</sup> This means that it tends to diffuse into the bulk; however, this is not expected to take place at the temperature of deposition, i.e., 298 K, because of kinetic limitations.<sup>28,29</sup> Despite this, we believe that exchange of Ru and Pt at the ad-island edges during growth is feasible because the energy required for this process to take place is lower; e.g., Ru surface exchange on Pt(111) starts at a temperature of at least 300–400 K lower than that for Ru bulk diffusion.<sup>29</sup> However, in the present case of Ru/Pt(332), it can be seen from STM images (Figure 3b) that the 2D ad-island edges are mainly constituted of Ru atoms, as occurs also for 1D structures. This is apparently in contradiction to reducing the surface energy.<sup>56</sup> However, considering that exchange processes have low incidence at room temperature even at the step edges, this suggests that the mixed 2D nanostructures are formed mainly due to some atomic exchange at the step edge or ad-island edge during initial growth (Figure 4C), followed by the incorporation of Ru ad-atoms diffusing from the lower terrace to the previously formed row. Thus, this last process is mainly responsible for 1D and 2D growth.

Finally, from the above discussion, the 1D chain structure and the mixed 2D ad-islands formation scenario for Ru deposited on Pt(332) can be outlined considering: (i) some atom exchange at the step edges and Ru ad-atoms incorporation to 1D or 2D structures occurring from the lower terrace and (Figures 4C and 4A, respectively), (ii) minor surface exchange of Ru ad-atoms with Pt atoms at the terrace occurring exclusively at ad-islands edges during growth, and (iii) exchange process at the terrace (Figure 4D) kinetically

hindered at 298 K and corner-diffusion process (Figure 4B) hindered after 2D growth begins. Thus, in this context, at low Ru coverage 1D and 2D (ad-islands) nanostructures grow attached to the step edges, some of them containing both Pt and Ru, as depicted in Figure 4E, where the black arrow and thicker atoms edges indicate the original position of the step edge.

As demonstrated, for Ru grown on the Pt(332) vicinal surface, the high density of defects changes the initial growth and final island shape when compared to smooth surfaces. The 1D and 2D smaller and elongated structures might influence catalytic activity and selectivity in a different way than that observed for more spherical and/or triangular/hexagonal larger islands grown on flat surfaces.<sup>29,30</sup> For instance, electrochemical experiments of CO stripping performed by Samjeské et al.<sup>33</sup> on Ru-decorated Pt(332) and (775) (both surfaces having six atoms terrace width and different step orientation) showed only one oxidation peak at low potential for the Ru-decorated Pt(332), in contrast to what is observed for smooth surfaces<sup>12,57</sup> and Ru-decorated Pt NPs with no high index surface planes,<sup>27</sup> where two oxidation peaks appear, arising from CO<sub>ads</sub> at the edges of Ru islands and Pt terrace sites distant from the islands, and a single broadened peak is observed on smooth surfaces and NPs only for higher Ru coverage.<sup>8,27</sup>

**High Coverage.** Figures 5a and 5b show STM images of the Ru/Pt(332) surfaces for  $\theta_{\text{Ru}} = 0.94$  ML and  $\theta_{\text{Ru}} = 1.48$  ML, along with a line profile for the islands. As can be seen, increasing coverage leads to the formation of bilayers, as determined from the height of the islands.

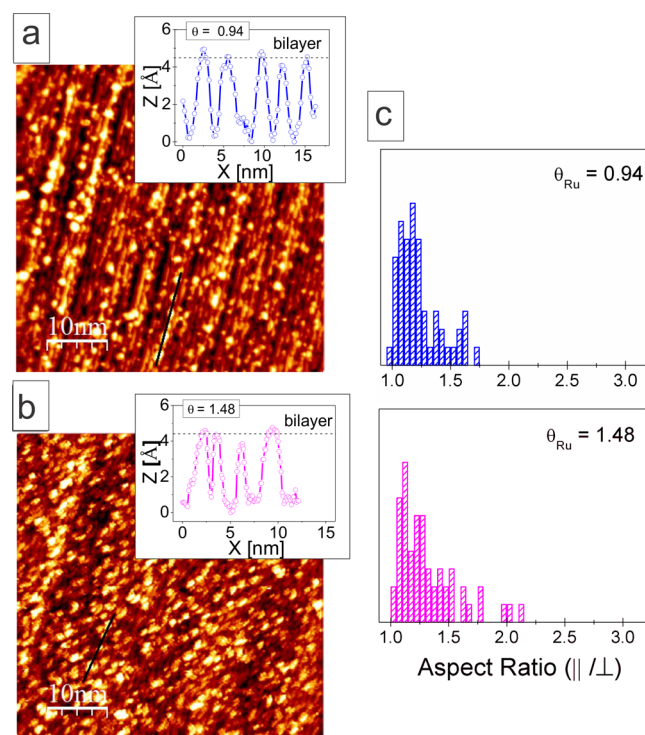


**Figure 5.** STM (50 nm × 50 nm) images at RT of (a) Ru<sub>0.94</sub>/Pt(332);  $U_b = 1.06$  V,  $I_t = 0.53$  nA and (b) Ru<sub>1.48</sub>/Pt(332);  $U_b = 1.05$  V,  $I_t = 0.25$  nA. Insets show the line profile of islands from (a) and (b). (c) Aspect ratio ( $\parallel/\perp$ ) frequency distribution of bilayer islands estimated from STM images. Coverage in ML indicated in the figure.

The bilayer growth behavior of Ru on Pt(111) was explained in terms of vertical ligand effect and lattice misfit.<sup>29,30</sup> Mainly, a stronger Ru–Ru interaction (weaker Ru interaction with the Pt(111) surface atoms) favors bilayer islands, where lattice misfit has a minor role.<sup>30</sup>

Once an ad-atom attaches to a step edge it can diffuse along the step edge, but it is unlikely to detach from it, unless temperature is high enough.<sup>48,50,58</sup> For Ru on Pt(111) the Ru mass transport between islands (which would require ad-atom detaching from a growing island) is not activated at temperatures under 500 K.<sup>30</sup> Thus, for the present system, having Pt(332) a larger amount of low-coordinated atoms and small terraces (high density of steps), it offers several preferred sites of nucleation where the Ru atoms will attach, delaying the beginning of a second layer growth over the step edge at the temperature of deposition. Therefore, islands with a bilayer height begin to form when the coverage increases, as depicted in Figure 6. In this sense, there may be a critical ad-island size

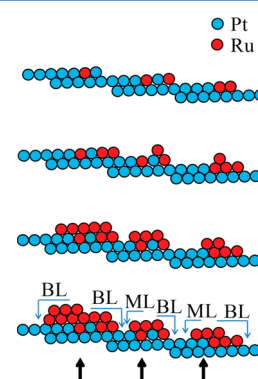


**Figure 6.** Schematic representation of Ru growth stages on a vicinal Pt surface. Blue arrows indicate monolayers (ML) and bilayers (BL) at the final stage. Black arrows show the position of the original step edges.

for the second layer to grow. For instance, Tersoff et al.<sup>59</sup> showed that there is a critical radius ( $R_c$ ) for a second layer to nucleate on top of the first layer as an island grows. Therefore, for Ru/Pt(332), for a coverage where the final island radius ( $R_f$ ) is  $R_f < R_c$ , islands with monolayer height would be expected. Consequently, increasing coverage can increase  $R_f$  to a value where  $R_f \geq R_c$  and a second layer on the islands begins to grow. Moreover, it has been shown that Ru (and Pt) ad-atoms at the outermost layer prefer adsorption on Ru<sub>3</sub> sites,<sup>31,32</sup> which could also have a key role for the beginning of the second layer growth on a vicinal surface. Additionally, if the second layer overgrows the upper terrace of the step edge, it can stabilize another layer above it.<sup>29</sup> Thus, the island would have, on each side of the step edge, a bilayer height with respect to the terrace underneath (as represented on the last stage of Ru growth in Figure 6). For Ru/Pt(332), the bilayer islands grow with no regular shape as can be seen from the STM images. Nevertheless, it can be seen that some islands are elongated along the step edges. To evaluate this, histograms of the aspect ratio (AR) for the bilayer islands are shown in Figure 5c. The AR is defined as the dimension of the island as measured parallel to the step edge divided that of the island as measured perpendicular to the step edge. Thus, a value for AR of 1 means a spherical shape, while values higher than 1 mean that the island has an elongated shape with the larger diameter being parallel to the step edge. As can be seen from Figure 5c, the

islands are slightly elongated, being the AR distribution narrower for the lowest coverage.

Brekó et al.<sup>29</sup> observed for Ru deposited on Pt(111) at 303 and 373 K small islands with no regular shape combined with larger triangular ones. The authors explained the absence of a regular shape by kinetic effects due to the high mobility of ad-atoms at steps and corners for small islands. For the Pt vicinal surface, Ru triangular islands are not observed, probably due to the small size of the terraces which confines the growth to a smaller dimension; thus, only small irregular islands are formed. Moreover, the high density of steps induces anisotropic growth, giving rise to a shape slightly elongated parallel to the steps.

It seems to be commonly accepted that the bifunctional mechanism is the significant factor for the improvement of methanol oxidation on Pt–Ru catalysts.<sup>13,24,60</sup> However, some authors believe that the electronic factor also has a major role.<sup>10,11,15,17,33,61</sup> The “ideal” atomic distribution of Ru and Pt over the catalysts’ surface is still unclear. Depending on the Pt:Ru composition and the procedure adopted to prepare Ru-decorated Pt(111) surfaces, reported results show both higher or lower methanol electrooxidation activity than that for Pt–Ru surface alloys, thus giving rise to different conclusions where the optimum atomic distribution can be considered to be that of the alloyed surfaces<sup>23</sup> or decorated surfaces.<sup>26</sup> However, it is accepted that for a higher CO and CH<sub>3</sub>OH electrooxidation activity there has to be a favorable relation of Ru–Pt edge sites that maximizes the intermetallic boundary region, i.e., small island growth.<sup>23,26,62</sup> Additionally, undercoordinated Ru ad-atoms have been considered to have a major role for the MOR.<sup>19,26,34,63</sup> It is worth noting that Ru decoration of a surface with high density of defects (as NPs or vicinal surfaces) would maximize the amount of low-coordinated Ru ad-atoms and minimize the island size, which would enhance the surface catalytic activity toward the MOR. Moreover, other factors such as shape of the islands formed could also be relevant. For instance, 2D nanostructures grow with no defined shape (rough), as shown here, and several kink sites develop, which will probably have an impact on the catalytic activity of the surface.

Liu et al.<sup>64</sup> found high activity for MOR with Ru-decorated tetrahedral (THH) Pt NPs. THH Pt nanocrystals are NPs bounded by well-defined high index crystal planes, namely (730) planes, which have terraces of 2 and 3 atoms width, having thus high density of low coordination surface Pt atoms. The stripping of CO recorded in H<sub>2</sub>SO<sub>4</sub> solution on this catalyst with  $\theta_{\text{Ru}} = 0.11$ – $0.53$  ML showed one oxidation peak. The authors deduced that only one peak was observed even at very low coverage due to the narrow terraces, since Ru atoms would decorate the step edges and thus CO<sub>ads</sub> would never be to distant from the Ru ad-atoms. Furthermore, the authors observed that the onset potential and peak potential for CO oxidation shifted to more negative values for the Ru decorated THH Pt NPs. This shift increases from  $\theta_{\text{Ru}} = 0.11$ – $0.32$  ML. For higher coverage, up to  $\theta_{\text{Ru}} = 0.53$  ML, the potential shift no longer increases and remains approximately constant.

The differences observed with the THH Pt NPs for lower and higher coverage can be related with our observations regarding the structure of deposits, which change with coverage. For instance, fully decorated steps of a (730) surface by 1D structures would require a coverage of  $\sim 0.43$  ML (if 1D structures decorate all steps before 2D structures start to form). Thus, it can be considered that the major potential shifts observed by the authors might occur when 1D structures grow

decorating the steps of the THH NPs’ surface ( $\theta_{\text{Ru}} \leq 0.32$  ML). For higher coverage ( $\theta_{\text{Ru}} = 0.42$ – $0.53$  ML), 2D (and maybe 3D) structures start to form, and this has no major effect over the onset and peak potential for CO oxidation when compared to  $\theta_{\text{Ru}} = 0.32$  ML. These can be attributed to the maximized amount of undercoordinated Ru atoms and intermetallic region for  $\theta_{\text{Ru}} = 0.32$  ML as 1D structures would decorate the steps. By increasing the Ru coverage 2D structures would form giving no additional undercoordinated Ru atoms and thus having no further improvement of the onset and peak potential for CO oxidation.

**Annealing Effect.** In order to study the behavior of the surface at higher temperature, all samples were thermally annealed at 623 K.

XPS showed no changes in the core-line intensities, indicating that no bulk alloying (bulk diffusion) occurs at the annealing temperature. Furthermore, the BE of both Pt 4f and Ru 3d remain unchanged after annealing (Figure 2S and Table 2S). Wakisaka et al.<sup>61</sup> observed a 0.39 eV BE positive shift of the Pt 4f core line for a Pt<sub>60</sub>Ru<sub>40</sub> alloy thick film grown on polycrystalline Au in UHV conditions. Thus, from the XPS results, from which information up to the fourth layer is obtained under the experimental conditions used (as calculated from NIST electron Inelastic-Mean-Free-Path Database v:1.2, in NIST Standard Reference Database 71),<sup>65</sup> we believe that as no BE changes are observed for neither Pt 4f nor Ru 3d core lines for the Ru/Pt(332), even though some exchange of Ru and Pt atoms between the topmost layers (surface alloying) is possible, only little intermixing between Ru and Pt occurs, and Ru diffusion does not occur beyond the second layer at the annealing temperature, in agreement with previously reported results for Ru on Pt(111).<sup>29,30</sup>

Figure 7 shows a STM image of the Ru <sub>$\theta=0.34$</sub> /Pt(332) after the thermal annealing. From the figure it can be seen that the

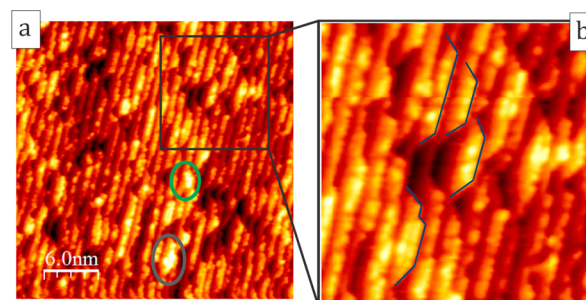


**Figure 7.** STM image at RT (30 nm × 30 nm) of the Ru <sub>$\theta=0.34$</sub> /Pt(332) annealed surface,  $U_b = 1.1$  V,  $I_t = 0.7$  nA (a) and an amplification showing the trapezoid shaped ad-islands (b).

ad-islands have more defined edges when compared to the initial surface (Figure 3), and although some bilayers can be detected (e.g., see green circle at Figure 7a), the majority of the ad-islands remain as monolayer (see Figure 5S). It must also be noted that occasionally a 3D trilayer (TL) might form (marked with a gray circle at Figure 7a) when the nanostructure overgrows two contiguous steps (Figure 6S).

The nanoislands’ structure developed during growth at a particular temperature will be mainly determined by the activation energy of atom diffusion processes and the surface morphology.<sup>48,58,66,67</sup> Jacobsen et al.<sup>67</sup> simulated island shapes as a function of temperature for the homoepitaxial growth on Pt(111) for the temperature range 245–790 K. They found



triangular island at 370 and 640 K (with different orientations) and hexagonal ones at 510 and 790 K. The authors discuss the different shapes considering the corner diffusion and edge diffusion processes<sup>53,66</sup> at and to the different step edges that emerge for islands grown on a (111) surface,<sup>67</sup> i.e., A-type edge, having (100) orientation at the step microfacet, and B-type edge, having (111) orientation at the step microfacet,<sup>50,53,67</sup> since the diffusion barriers can be different for each type of edge.<sup>53,54,58,66</sup>

For Ru grown on Pt(111) at different temperatures in the range 303–773 K, island shape was observed to change from triangular to hexagonal with UHV-STM.<sup>29</sup> In the temperature range 623–673 K, islands with a distorted hexagonal shape and monolayer height were observed. In this case the authors attributed this fact to the increasing rate of vertical exchange processes between Ru and Pt atoms, changing the composition of the island and the underlying substrate layer, as confirmed by STM and AES. Moreover, Hoster et al.<sup>26</sup> observed hexagonal islands after annealing at 820 K a sputtered Pt(111) surface where Ru was deposited from the vapor phase.

From this it could be expected for the Ru ad-islands grown on Pt(332) to change their shape into a more regular one after annealing and to behave in a similar way as Ru on smooth Pt(111). From Figure 7b, it can be seen that the ad-islands adopt a shape that resembles part of a (quasi)hexagon. Probably, completely hexagonal islands are unlikely to form due to the small terrace size, and instead, influenced by the high density of steps, ad-islands grow with trapezoid shape (as depicted with blue lines over the image) attached to the steps. Therefore, in the case of a vicinal surface, not only the diffusion limiting processes but also the surface stepped nature will dictate the morphology of the islands growth (e.g., anisotropic induced growth and confined growth), as discussed before, and probably the thermodynamically stable preferred shape.

Unfortunately, a good chemical contrast for the STM images of the annealed sample was not achieved, it being impossible to clearly distinguish between Ru and Pt atoms after the annealing. However, as the ad-islands remain as monolayer (Figure 5S) the differences in brightness can be attributed to the composition, and thus, from the image in Figure 7 it can be assumed that Ru atoms are mainly at the ad-islands and ad-island step edges. Probably, at the annealing temperature diffusion along the step edges and corner-diffusion processes are already activated, but diffusion of Ru perpendicularly to the step edges is not; hence, it remains mainly at the ad-islands surface, and it is not likely to observe Ru on the original Pt terraces surface. Moreover, considering this diffusion processes, the elongated shapes at the annealing temperature can also be explained. Finally, a slight increase of the bilayer islands (3D nanostructures) can be expected since at 623 K the interlayer diffusion from the first to the second layer is already activated.<sup>30</sup>

Figures 8a and 8b show STM images of the annealed surfaces for  $\theta_{\text{Ru}} = 0.94$  ML and  $\theta_{\text{Ru}} = 1.48$  ML. The shape of the bilayer islands is still irregular after the annealing procedure, in contrast to what is observed at lower coverage for the monolayer ad-islands, and also different than the reported triangular shape for bilayer islands of Ru on Pt(111) after annealing at 490 K.<sup>30</sup>

The main difference between low and high coverage for Pt(332) is that the ad-islands at low coverage have monolayer height and grow attached to a continuous step, while at the bilayer islands the second layer is not attached to a continuous step. In this sense, for the monolayer ad-island the diffusion along the step and corner-diffusion processes can account for

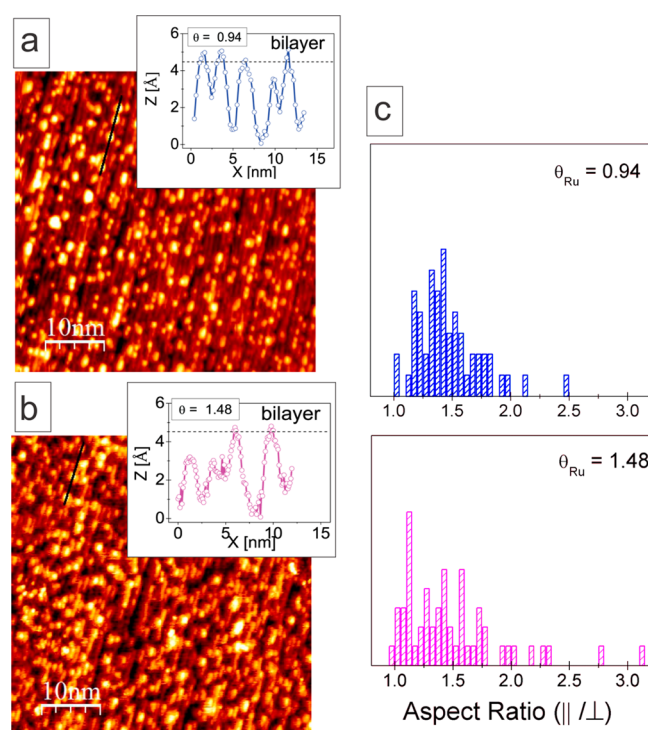


**Figure 8.** STM images (50 nm × 50 nm) at RT of the (a) Ru<sub>0.94</sub>/Pt(332),  $U_b = 1.05$  V,  $I_t = 0.38$  nA and (b) Ru<sub>1.48</sub>/Pt(332),  $U_b = 1.06$  V,  $I_t = 0.35$  nA. Insets show the line profile of islands from (a) and (b). (c) Aspect ratio ( $\parallel/\perp$ ) frequency distribution of 3D islands for the annealed surfaces estimated from STM images. Coverage in ML indicated in the figure.

the shape change. In addition, the second layer at the bilayer would have to increase its size in order to have more defined edges since, as previously mentioned, small islands tend to have irregular shape due to the high mobility of ad-atoms at the edges and corners.<sup>29,58</sup>

Figure 8c shows the AR of the 3D islands. It is worth noting that after annealing there is a wider distribution of ARs. Also, in both cases AR increases with annealing, indicating that 3D nanostructures become slightly more elongated. This could be due to an increase of the number of bilayer islands caused by the annealing. Annealing a Ru/Pt(111) surface at 400 K already promotes an increase of the amount of bilayer islands because of the activation of interlayer mass transport within an island,<sup>30</sup> driving Ru atoms to “hop” onto the second layer.<sup>29,30</sup> For Ru on Pt(332) annealed at 623 K it can be considered that this also takes place. Thus, Ru atoms of the first layer go onto the second layer. To evaluate this argument, the percentage of area occupied by 3D islands with respect to the total surface area was estimated from the STM images before and after annealing for all coverage (shown in Figure 8S). There is a clear tendency of increasing 3D islands percentage upon annealing, in agreement with increasing bilayer formation.

Differences found between catalytic activity of Ru-decorated Pt NPs and low-Miller-index single crystals can be associated not only to the dimensions of the NPs but also to the different nanostructures formed after surface decoration due to the high density of low coordinated atoms at NPs surfaces. It seems clear that the cluster size, shape, distribution (island–island distance), and density of defects can influence the electrocatalytic activity; being these features especially important in the case of decorated surfaces.<sup>6,23,33,68</sup> Structure analysis (as by



UHV-STM) becomes crucial to associate differences in catalytic activity with surface modifications, since coverage can also influence the nanoislands' structure.

Finally, from the arguments presented in this article, we believe that using vicinal surfaces as new model systems for studying the structure–reactivity relation with a surface science approach will bring new insights for the understanding of the catalytic activity of Pt–Ru systems, such as core–shell type NPs and particularly for the more recent Ru/Pt NPs of high-index surfaces, which have shown higher catalytic activity, and hopefully this would help to comprehend unanswered questions, which will lead to the design of novel and better catalysts for fuel cell applications.

## CONCLUSIONS

We have demonstrated that Ru can be grown as 1D and 2D nanostructures on a vicinal Pt surface. These 1D and 2D structures grow exclusively decorating the step edges. For low coverage, 2D nanostructures grow with irregular shape and adopt a trapezoid shape when the surface is annealed at 623 K. The 3D bilayer growth is delayed due to the stepped nature of the Pt(332) surface and sets in for higher coverage, probably as a result of a minimum width (or critical radius) for the 2D ad-island to stabilize a second Ru layer. Also, annealing at 623 K induces some 3D growth due to interlayer mass transport between the islands layers. 3D nanostructures have irregular shape even after annealing, due to their small size. These structures have slightly elongated shape due to the high density of steps of the underlying Pt substrate which induces anisotropic growth, which is further favored upon annealing.

XPS showed that BE of the Ru nanostructures is independent of coverage. Whether for Pt or for Ru, the core-line intensity and BE remained unchanged after annealing, indicating no bulk alloying (bulk diffusion), whereas surface alloy formation is possible in the topmost layers.

Finally, our findings bring new insights into the differences in electrocatalytic activity behavior reported for Ru-decorated Pt smooth and vicinal single crystals and also NPs systems and help explain tendencies observed for decorated NPs. Thus, we believe that decorated-vicinal surfaces as new model systems can help to fill the gap between single crystals and NPs, especially considering the recent advances in producing NPs with high density of low-coordinated atoms (vicinal NPs).

## ASSOCIATED CONTENT

### Supporting Information

Additional information, XPS fitting details, STM images, and figures. This material is available free of charge via the Internet at <http://pubs.acs.org>.

## AUTHOR INFORMATION

### Corresponding Authors

\*(E.A.C.) Tel +55 (19) 35215334; e-mail [emiliacarbonio@gmail.com](mailto:emiliacarbonio@gmail.com).

\*(M.J.P.) Tel +55 (19) 35215334; e-mail [prietomauricio@gmail.com](mailto:prietomauricio@gmail.com).

### Notes

The authors declare no competing financial interest.

## ACKNOWLEDGMENTS

Authors acknowledge financial support from FAPESP (proc.07/54829-5) and CNPq. EAC and MJP acknowledge

fellowships granted from CNPq (proc. 150192/2014-2) and FAPESP (proc. 2011/12566-3).

## ABBREVIATIONS

PEMFC, polymer electrolyte membrane fuel cell; DMFC, direct methanol fuel cell; MOR, methanol oxidation reaction; RT, room temperature.

## REFERENCES

- (1) Solla-Gullon, J.; Vidal-Iglesias, F. J.; Feliu, J. M. Shape Dependent Electrocatalysis. *Annu. Rep. Prog. Chem., Sect. C: Phys. Chem.* **2011**, *107*, 263–297.
- (2) Housmans, T. H. M.; Koper, M. T. M. Methanol Oxidation on Stepped Pt[N(111) X (110)] Electrodes: A Chronoamperometric Study. *J. Phys. Chem. B* **2003**, *107*, 8557–8567.
- (3) Shin, J. W.; Korzeniewski, C. Infrared Spectroscopic Detection of Co Formed at Step and Terrace Sites on a Corrugated Electrode Surface Plane during Methanol Oxidation. *J. Phys. Chem.* **1995**, *99*, 3419–3422.
- (4) Markovic, N. M.; Gasteiger, H. A.; Ross, P. N. Oxygen Reduction on Platinum Low-Index Single-Crystal Surfaces in Sulfuric-Acid-Solution - Rotating Ring-Pt(hkl) Disk Studies. *J. Phys. Chem.* **1995**, *99*, 3411–3415.
- (5) Markovic, N. M.; Schmidt, T. J.; Stamenkovic, V.; Ross, P. N. Oxygen Reduction Reaction on Pt and Pt Bimetallic Surfaces: A Selective Review. *Fuel Cells* **2001**, *1*, 105–116.
- (6) Ehteshami, S. M. M.; Chan, S. H. A Review of Electrocatalysts with Enhanced Co Tolerance and Stability for Polymer Electrolyte Membrane Fuel Cells. *Electrochim. Acta* **2013**, *93*, 334–345.
- (7) Liu, H. S.; Song, C. J.; Zhang, L.; Zhang, J. J.; Wang, H. J.; Wilkinson, D. P. A Review of Anode Catalysis in the Direct Methanol Fuel Cell. *J. Power Sources* **2006**, *155*, 95–110.
- (8) Petrii, O. A. Pt-Ru Electrocatalysts for Fuel Cells: A Representative Review. *J. Solid State Electrochem.* **2008**, *12*, 609–642.
- (9) Iwasita, T. Electrocatalysis of Methanol Oxidation. *Electrochim. Acta* **2002**, *47*, 3663–3674.
- (10) Christoffersen, E.; Liu, P.; Ruban, A.; Skriver, H. L.; Norskov, J. K. Anode Materials for Low-Temperature Fuel Cells: A Density Functional Theory Study. *J. Catal.* **2001**, *199*, 123–131.
- (11) Bligaard, T.; Norskov, J. K. Ligand Effects in Heterogeneous Catalysis and Electrochemistry. *Electrochim. Acta* **2007**, *52*, 5512–5516.
- (12) Spendelow, J. S.; Babu, P. K.; Wieckowski, A. Electrocatalytic Oxidation of Carbon Monoxide and Methanol on Platinum Surfaces Decorated with Ruthenium. *Curr. Opin. Solid State Mater. Sci.* **2005**, *9*, 37–48.
- (13) Lu, C.; Masel, R. I. The Effect of Ruthenium on the Binding of CO, H<sub>2</sub>, and H<sub>2</sub>O on Pt(110). *J. Phys. Chem. B* **2001**, *105*, 9793–9797.
- (14) Watanabe, M.; Motoo, S. Electrocatalysis by Ad-Atoms. 3. Enhancement of Oxidation of Carbon-Monoxide on Platinum by Ruthenium Ad-Atoms. *J. Electroanal. Chem.* **1975**, *60*, 275–283.
- (15) Godoi, D. R. M.; Perez, J.; Villulas, H. M. Effects of Alloyed and Oxide Phases on Methanol Oxidation of Pt-Ru/C Nanocatalysts of the Same Particle Size. *J. Phys. Chem. C* **2009**, *113*, 8518–8525.
- (16) Godoi, D. R. M.; Perez, J.; Villulas, H. M. Influence of Particle Size on the Properties of Pt-Ru/C Catalysts Prepared by a Microemulsion Method. *J. Electrochem. Soc.* **2007**, *154*, B474–B479.
- (17) Godoi, D. R. M.; Villulas, H. M. Relevance of Electronic Effects on the Yield of CO<sub>2</sub> from Methanol Oxidation. *Langmuir* **2012**, *28*, 1064–1067.
- (18) Rigsby, M. A.; Zhou, W. P.; Lewera, A.; Duong, H. T.; Bagus, P. S.; Jaegermann, W.; Hunger, R.; Wieckowski, A. Experiment and Theory of Fuel Cell Catalysis: Methanol and Formic Acid Decomposition on Nanoparticle Pt/Ru. *J. Phys. Chem. C* **2008**, *112*, 15595–15601.
- (19) Waszczuk, P.; Solla-Gullon, J.; Kim, H. S.; Tong, Y. Y.; Montiel, V.; Aldaz, A.; Wieckowski, A. Methanol Electrooxidation on Platinum/Ruthenium Nanoparticle Catalysts. *J. Catal.* **2001**, *203*, 1–6.

- (20) Wang, J.-J.; Liu, Y.-T.; Chen, I. L.; Yang, Y.-W.; Yeh, T.-K.; Lee, C. H.; Hu, C.-C.; Wen, T.-C.; Chen, T.-Y.; Lin, T.-L. Near-Monolayer Platinum Shell on Core–Shell Nanocatalysts for High-Performance Direct Methanol Fuel Cell. *J. Phys. Chem. C* **2014**, *118*, 2253–2262.
- (21) Iwasita, T.; Vielstich, W. Online Mass-Spectroscopy of Volatile Products during Methanol Oxidation at Platinum in Acid-Solutions. *J. Electroanal. Chem.* **1986**, *201*, 403–408.
- (22) Iwasita, T.; Nart, F. C.; Vielstich, W. An FTIR Study of the Catalytic Activity of a 85–15 Pt–Ru Alloy for Methanol Oxidation. *Ber. Bunsen-Ges. Phys. Chem.* **1990**, *94*, 1030–1034.
- (23) Iwasita, T.; Hoster, H.; John-Anacker, A.; Lin, W. F.; Vielstich, W. Methanol Oxidation on PtRu Electrodes. Influence of Surface Structure and Pt–Ru Atom Distribution. *Langmuir* **2000**, *16*, 522–529.
- (24) Lu, C.; Rice, C.; Masel, R. I.; Babu, P. K.; Waszczuk, P.; Kim, H. S.; Oldfield, E.; Wieckowski, A. UHV, Electrochemical NMR, and Electrochemical Studies of Platinum/Ruthenium Fuel Cell Catalysts. *J. Phys. Chem. B* **2002**, *106*, 9581–9589.
- (25) Tritsarlis, G. A.; Rossmeisl, J. Methanol Oxidation on Model Elemental and Bimetallic Transition Metal Surfaces. *J. Phys. Chem. C* **2012**, *116*, 11980–11986.
- (26) Hoster, H.; Iwasita, T.; Baumgartner, H.; Vielstich, W. Pt–Ru Model Catalysts for Anodic Methanol Oxidation: Influence of Structure and Composition on the Reactivity. *Phys. Chem. Chem. Phys.* **2001**, *3*, 337–346.
- (27) Maillard, F.; Lu, G. Q.; Wieckowski, A.; Stimming, U. Ru-Decorated Pt Surfaces as Model Fuel Cell Electrocatalysts for CO Electrooxidation. *J. Phys. Chem. B* **2005**, *109*, 16230–16243.
- (28) Hoster, H. E.; Bergbreiter, A.; Erne, P. M.; Hager, T.; Rauscher, H.; Behm, R. J. Pt<sub>(x)</sub>Ru<sub>(1-x)</sub>/Ru(0001) Surface Alloys - Formation and Atom Distribution. *Phys. Chem. Chem. Phys.* **2008**, *10*, 3812–3823.
- (29) Berko, A.; Bergbreiter, A.; Hoster, H. E.; Behm, R. J. From Bilayer to Monolayer Growth: Temperature Effects in the Growth of Ru on Pt(111). *Surf. Sci.* **2009**, *603*, 2556–2563.
- (30) Bergbreiter, A.; Berko, A.; Erne, P. M.; Hoster, H. E.; Behm, R. J. On the Origin of Ru Bilayer Island Growth on Pt(111). *Vacuum* **2009**, *84*, 13–18.
- (31) Diemant, T.; Bergbreiter, A.; Bansmann, J.; Hoster, H. E.; Behm, R. J. From Adlayer Islands to Surface Alloy: Structural and Chemical Changes on Bimetallic PtRu(0001) Surfaces. *ChemPhysChem* **2010**, *11*, 3123–3132.
- (32) Bergbreiter, A.; Hoster, H. E.; Behm, R. J. Segregation and Stability in Surface Alloys: Pd<sub>x</sub>Ru<sub>1-x</sub>/Ru(0001) and Pt<sub>x</sub>Ru<sub>1-x</sub>/Ru(0001). *ChemPhysChem* **2011**, *12*, 1148–1154.
- (33) Samjeske, G.; Xiao, X. Y.; Baltruschat, H. Ru Decoration of Stepped Pt Single Crystals and the Role of the Terrace Width on the Electrocatalytic CO Oxidation. *Langmuir* **2002**, *18*, 4659–4666.
- (34) Wang, H. S.; Baltruschat, H. Dens Study on Methanol Oxidation at Poly- and Monocrystalline Platinum Electrodes: The Effect of Anion, Temperature, Surface Structure, Ru Adatom, and Potential. *J. Phys. Chem. C* **2007**, *111*, 7038–7048.
- (35) Mugarza, A.; Ortega, J. E. Electronic States at Vicinal Surfaces. *J. Phys.: Condens. Matter* **2003**, *15*, S3281–S3310.
- (36) Gambardella, P.; Kern, K. Ni Growth on Vicinal Pt(111): Low Temperature Exchange and Formation of Ordered Surface Alloys. *Surf. Sci.* **2001**, *475*, L229–L234.
- (37) Prieto, M. J.; Carbonio, E. A.; Fatayer, S.; Landers, R.; de Siervo, A. Electronic and Structural Study of Pt-Modified Au Vicinal Surfaces: A Model System for Pt–Au Catalysts. *Phys. Chem. Chem. Phys.* **2014**, *16*, 13329–13339.
- (38) Wu, B. H.; Zheng, N. F. Surface and Interface Control of Noble Metal Nanocrystals for Catalytic and Electrocatalytic Applications. *Nano Today* **2013**, *8*, 168–197.
- (39) Lee, K.; Kim, M.; Kim, H. Catalytic Nanoparticles Being Facet-Controlled. *J. Mater. Chem.* **2010**, *20*, 3791–3798.
- (40) Kim, D. Y.; Im, S. H.; Park, O. O. Synthesis of Tetrahedral Gold Nanocrystals with High-Index Facets. *Cryst. Growth Des.* **2010**, *10*, 3321–3323.
- (41) Xia, B. Y.; Wu, H. B.; Wang, X.; Lou, X. W. Highly Concave Platinum Nanoframes with High-Index Facets and Enhanced Electrocatalytic Properties. *Angew. Chem., Int. Ed.* **2013**, *52*, 12337–12340.
- (42) Tian, N.; Zhou, Z. Y.; Sun, S. G. Platinum Metal Catalysts of High-Index Surfaces: From Single-Crystal Planes to Electrochemically Shape-Controlled Nanoparticles. *J. Phys. Chem. C* **2008**, *112*, 19801–19817.
- (43) Horcas, I.; Fernandez, R.; Gomez-Rodriguez, J. M.; Colchero, J.; Gomez-Herrero, J.; Baro, A. M. WSXM: A Software for Scanning Probe Microscopy and a Tool for Nanotechnology. *Rev. Sci. Instrum.* **2007**, *78*, 013705–8.
- (44) Clavilier, J.; El Achi, K.; Rodes, A. In Situ Probing of Step and Terrace Sites on Pt(S)-[N(111) × (111)] Electrodes. *Chem. Phys.* **1990**, *141*, 1–14.
- (45) Moulder, J. F.; Stickle, W. F.; Sobol, P. E.; Bomben, K. D. *Handbook of X Ray Photoelectron Spectroscopy: A Reference Book of Standard Spectra for Identification and Interpretation of XPS Data*; PerkinElmer Corp.: Waltham, MA, 1995.
- (46) Cramm, S.; Friedrich, K. A.; Geyzers, K. P.; Stimming, U.; Vogel, R. Surface Structural and Chemical Characterization of Pt/Ru Composite Electrodes: A Combined Study by XPS, STM and IR Spectroscopy. *Fresenius J. Anal. Chem.* **1997**, *358*, 189–192.
- (47) Schmid, M.; Varga, P. Segregation and Surface Chemical Ordering—an Experimental View on the Atomic Scale. In *The Chemical Physics of Solid Surfaces*; Woodruff, D. P., Ed.; Elsevier: Amsterdam, 2002; Vol. 10, pp 118–151.
- (48) Tsong, T. T.; Chen, C. Dynamics and Diffusion of Atoms at Stepped Surfaces. In *The Chemical Physics of Solid Surfaces*; King, D. A., Woodruff, D. P., Eds.; Elsevier: Amsterdam, 1997; Vol. 8, pp 102–148.
- (49) Zhang, Z.; Lagally, M. G. Atomistic Processes in the Early Stages of Thin-Film Growth. *Science* **1997**, *276*, 377–383.
- (50) Kuhnke, K.; Kern, K. Vicinal Metal Surfaces as Nanotemplates for the Growth of Low-Dimensional Structures. *J. Phys.: Condens. Matter* **2003**, *15*, S3311–S3335.
- (51) Brune, H. Microscopic View of Epitaxial Metal Growth: Nucleation and Aggregation. *Surf. Sci. Rep.* **1998**, *31*, 121–229.
- (52) Iwasita, T.; Schmickler, W.; Schultze, J. W. The Influence of Metal Adatoms Deposited at Underpotential on the Kinetics of an Outer-Sphere Redox Reaction. *J. Electroanal. Chem.* **1985**, *194*, 355–359.
- (53) Leonardelli, G.; Lundgren, E.; Schmid, M. Adatom Interlayer Diffusion on Pt(111): An Embedded Atom Method Study. *Surf. Sci.* **2001**, *490*, 29–42.
- (54) Maca, F.; Kotrla, M.; Trushin, O. S. Energy Barriers for Diffusion on Stepped Pt(111) Surface. *Vacuum* **1999**, *54*, 113–117.
- (55) Maca, F.; Kotrla, M.; Trushin, O. S. Energy Barriers for Diffusion on Stepped Rh(111) Surfaces. *Surf. Sci.* **2000**, *454*, 579–583.
- (56) Ruban, A. V.; Skriver, H. L.; Nørskov, J. K. Surface Segregation Energies in Transition-Metal Alloys. *Phys. Rev. B* **1999**, *59*, 15990–16000.
- (57) Spendelow, J. S.; Wieckowski, A. Noble Metal Decoration of Single Crystal Platinum Surfaces to Create Well-Defined Bimetallic Electrocatalysts. *Phys. Chem. Chem. Phys.* **2004**, *6*, 5094–5118.
- (58) Jacobsen, J.; Jacobsen, K. W.; Stoltze, P.; Nørskov, J. K. Island Shape-Induced Transition from 2d to 3d Growth for Pt/Pt(111). *Phys. Rev. Lett.* **1995**, *74*, 2295–2298.
- (59) Tersoff, J.; Vandergon, A. W. D.; Tromp, R. M. Critical Island Size for Layer-by-Layer Growth. *Phys. Rev. Lett.* **1994**, *72*, 266–269.
- (60) Yajima, T.; Uchida, H.; Watanabe, M. In-Situ ATR-FTIR Spectroscopic Study of Electro-Oxidation of Methanol and Adsorbed CO at Pt–Ru Alloy. *J. Phys. Chem. B* **2004**, *108*, 2654–2659.
- (61) Wakisaka, M.; Mitsui, S.; Hirose, Y.; Kawashima, K.; Uchida, H.; Watanabe, M. Electronic Structures of Pt–Co and Pt–Ru Alloys for CO-Tolerant Anode Catalysts in Polymer Electrolyte Fuel Cells Studied by EC–XPS. *J. Phys. Chem. B* **2006**, *110*, 23489–23496.
- (62) Rau, M. S.; de Chialvo, M. R. G.; Chialvo, A. C. Effect of the Pt/Ru Intermetallic Boundary on the Carbon Monoxide Electrooxidation: Excess Electrocatalytic Activity. *J. Power Sources* **2012**, *216*, 464–470.

(63) Perez, A.; Vilkas, M. J.; Cabrera, C. R.; Ishikawa, Y. Density Functional Theory Study of Water Activation and COads + OHads Reaction on Pure Platinum and Bimetallic Platinum/Ruthenium Nanoclusters. *J. Phys. Chem. B* **2005**, *109*, 23571–23578.

(64) Liu, H. X.; Tian, N.; Brandon, M. P.; Zhou, Z. Y.; Lin, J. L.; Hardacre, C.; Lin, W. F.; Sun, S. G. Tetrahedral Pt Nanocrystal Catalysts Decorated with Ru Adatoms and Their Enhanced Activity in Methanol Electrooxidation. *ACS Catal.* **2012**, *2*, 708–715.

(65) NIST electron Inelastic-Mean-Free-Path Database v:1.2, NIST Standard Reference Database 71.

(66) Brune, H.; Roder, H.; Bromann, K.; Kern, K.; Jacobsen, J.; Stoltze, P.; Jacobsen, K.; Norskov, J. Anisotropic Corner Diffusion as Origin for Dendritic Growth on Hexagonal Substrates. *Surf. Sci.* **1996**, *349*, L115–L122.

(67) Jacobsen, J.; Jacobsen, K. W.; Norskov, J. K. Simulations of Homoepitaxial Growth of Pt(111): Island Shapes and the Growth Mode. *Scanning Microsc.* **1998**, *12*, 81–91.

(68) Koper, M. T. M.; Lukkien, J. J.; Jansen, A. P. J.; van Santen, R. A. Lattice Gas Model for CO Electrooxidation on Pt-Ru Bimetallic Surfaces. *J. Phys. Chem. B* **1999**, *103*, 5522–5529.